Published in final edited form as:
Lasers Surg Med. 2012 October ; 44(8): 603–610. doi:10.1002/lsm.22070.

In vivo Imaging of Photoreceptor Disruption Associated with Age-Related Macular Degeneration: A Pilot Study

Adam Boretsky, BS[1,2], **Faraz Khan, BS**[1], **Garrett Burnett, BS**[3], **Daniel X. Hammer, PhD**[4], **R. Daniel Ferguson, MS**[4], **Frederik van Kuijk, MD, PhD**[5], and **Massoud Motamedi, PhD**[1,6]

[1]Center for Biomedical Engineering, University of Texas Medical Branch, Galveston, TX 77555, USA

[2]Human Pathophysiology and Translational Medicine, University of Texas Medical Branch, Galveston, TX 77555, USA

[3]School of Medicine, University of Texas Medical Branch, Galveston, TX 77555, USA

[4]Physical Sciences Inc., 20 New England Business Center, Andover MA 01810, USA

[5]Department of Ophthalmology, University of Minnesota, Minneapolis, MN 55455, USA

[6]Department of Ophthalmology and Visual Sciences, University of Texas Medical Branch, Galveston, TX 77555, USA

Abstract

Background and Objective—Age-related macular degeneration is one of the leading causes of vision loss in the developed world. As the disease progresses, the central part of the retina, called the macula, is compromised leading to a disruption of both structure and visual function. In this study, we investigate the disruption of macular photoreceptor cells *in vivo* as a function of disease stage in patients with the dry form of age-related macular degeneration AMD.

Materials and Methods—An investigational confocal Adaptive Optics Scanning Laser Ophthalmoscope (AO-SLO) was used to obtain high resolution images of the macular photoreceptor mosaic in patients previously diagnosed with AMD. Four patients were selected as representative cases, comprising each of the four clinical stages of AMD progression.

Results—AO-SLO imaging revealed slight disruption in the photoreceptor mosaic in early stage AMD due to focal drusen formation and identified several small drusen deposits that were not observed with standard clinical imaging techniques. An increase in photoreceptor disruption was visualized within the macula in direct correlation with the stage of AMD progression leading to a decrease in visual acuity. Large coalescent drusen and areas of geographic atrophy in advanced stage dry AMD exhibited a significant decrease in visible photoreceptor density. Significant decrease in photoreceptor counts (~35–50%) were observed when comparing earlier stages of AMD progression (Category I & II) to later stages of the disease (Category III & IV).

Conclusions—This study demonstrates the capabilities of adaptive optics retinal imaging to monitor disruption of individual photoreceptor cells as a function of disease progression yielding valuable diagnostic findings in early stage AMD beyond what can be learned about the health of photoreceptors using conventional retinal imaging techniques.

Address correspondence to: Massoud Motamedi, Ph.D., University of Texas Medical Branch, 301 University Blvd., Galveston, TX 77555-1156, Phone: (409) 772-8363, Fax: (409) 772-0751, mmotamed@utmb.edu.

Conflict of Interest Disclosure †DXH & RDF have a financial interest in adaptive optics technology through patents held by Physical Sciences Inc.

Keywords

Adaptive Optics; AMD; Drusen; Fundus Reflectance; Retina; Retinal Pigment Epithelium; SLO

Introduction

Age-related macular degeneration (AMD) is one of the most prevalent causes of visual impairment throughout the world and is expected to increase significantly over the next 40 years(1). The most common form of the disease “dry” AMD, represents 85–90% of all AMD cases(2). Unfortunately, there are no treatment options available for dry AMD. As the disease progresses, extracellular deposits called drusen form beneath the retinal pigment epithelium (RPE) which disrupt the overlying photoreceptor cells. These subtle changes often occur gradually and result in decreased central visual acuity. Clinically, drusen represent one of the earliest biomarkers of AMD, and progression of the disease is categorized primarily based on the size, shape, and location of this cellular debris within the macula. Abnormalities in the RPE may also accompany drusen and appear as either localized hyper- or hypo-pigmented spots(3). The advanced stage of dry AMD, Geographic Atrophy (GA), is characterized by the progressive loss of the RPE cells, the outer neurosensory retina and the choriocapillaris(4,5). Figure 1 depicts the progression of AMD and its impact on the RPE and photoreceptors. Degeneration of photoreceptor cells throughout the macula results in functional deficits leading to severe loss of central vision(6,7). The pathogenesis of AMD is still largely unknown, but there are multiple genetic and environmental factors that contribute to both the onset and progression of the disease. A greater understanding of the early alterations in retinal tissue may provide further insight into the mechanism(s) of disease progression and identify new approaches for therapeutic intervention.

High resolution retinal imaging systems have become prominent fixtures in the field of ophthalmology as powerful diagnostic tools. However, achieving detailed images of cellular structures within the retina using conventional ophthalmic techniques is limited by optical aberrations produced by ocular tissue, primarily the cornea and lens. Many of these aberrations can be overcome using emerging adaptive optics (AO) retinal imaging techniques to generate a clearer view of retinal morphology. AO imaging systems traditionally consist of 3 principal components which actively measure and correct optical aberrations to achieve heightened clarity and resolution. The three primary components of traditional AO systems are (1) a wavefront sensor (2) a corrective optical element and (3) a feedback control system(8). The wavefront sensor uses a lenslet array and a CCD camera to continuously measure distortions in the intensity and shape of the wavefront. The corrective optical element, generally a deformable mirror, compensates for optical aberrations by modifying the shape of the reflective surface. Finally, a software control system is used as an interface between the wavefront sensor and the corrective optical element. Since the first demonstration of AO enhanced retinal imaging nearly 15 years ago(9), these techniques have been successfully incorporated into a variety of retinal imaging systems, including a fundus camera, scanning laser ophthalmoscope (SLO)(10–12) and optical coherence tomography (OCT)(13,14). Recently, multiple retinal imaging techniques have been combined with AO(15,16).

Adaptive optics retinal imaging systems are currently limited to investigational use but show promise as an enhanced diagnostic imaging technique in the field of ophthalmology. Numerous studies have characterized the distribution of photoreceptors associated with aging and AMD based on histopathology. Recently, AO imaging has been used to assess the variation in cone photoreceptor density in healthy populations based on multiple parameters

such as age(17), eccentricity(18), eye length(19) and refractive error(20). By providing cellular resolution of retinal pathology *in vivo*, AO enhanced imaging may help guide future treatment strategies for numerous retinal diseases. This study was designed to examine each clinical stage of dry AMD with a multimodal clinical imaging system and an adaptive optics scanning laser ophthalmoscope (AO-SLO) to determine the integrity of the macular photoreceptors.

Materials and Methods

This study adhered to a protocol approved by the University of Texas Medical Branch Institutional Review Board and complied with all requirements of the Declaration of Helsinki. All patients provided informed consent prior to participation.

Patients

Four patients were recruited from the University of Texas Medical Branch Eye Center in Galveston, TX for this pilot study. Each patient had been previously diagnosed with AMD. The patients were selected as representative cases based on their respective category of AMD progression as outlined in the Age-Related Eye Disease Study (AREDS)(21). A brief description of the criteria for these categories may be found in Table 1. Exclusion criteria included retinal complications from diabetes mellitus, cataracts, or any other history of retinal surgery with the exception of intraocular lens (IOL) implantation. The participants in this study ranged in age from 65 – 86 years with a mean age of 75 years with a standard deviation of 8.7 years. Following a clinical examination, one eye from each patient was selected for further evaluation using the investigational AO-SLO. A summary of the patient demographics is provided in Table 2.

Imaging

Prior to the imaging examination, each patient received dilating eye drops (1% Tropicamide, Bausch & Lomb) to prevent accommodation of the pupil. A series of wide-field fundus reflectance images (30° × 30°, λ = 830 nm, 1536×1536 pixel resolution), fundus autofluorescence images (excitation λ = 488 nm; emission λ> 500 nm) and spectral domain optical coherence tomography cross-sections (SD-OCT, λ = 870 nm; acquisitionspeed, 40 000 A-scans per seconds; axial resolution ~7 μm; lateral optical resolution ~14 μm) were obtained with a multimodal clinical imaging system (Spectralis™, Heidelberg Engineering, Heidelberg, Germany). Multiple image frames were averaged during acquisition using the TruTrack™ active retinal tracking system to compensate for eye motion. These images were used to identify specific regions of interest and subsurface features to be evaluated with AO-SLO.

The custom built AO-SLO (Physical Sciences Inc., Andover, MA) was used to acquire high resolution images of the macular photoreceptor mosaic. The imaging and wavefront sensing light source for the AO-SLO was a superluminescent diode (SLD, Superlum, Moscow, Russia) centered at 830 nm with a bandwidth of 62 nm. A schematic of the optical layout of the AO-SLO is presented in Figure 2. The Shack-Hartmann wavefront sensor is a combination of a lenslet array (SussMicroOptics, Neuchatel, Switzerland) and a CCD camera (Uniq Vision Inc., Santa Clara, CA) that actively provides wavefront measurements across the pupil. A large stroke deformable mirror (Mirao 52d, Imagine Eyes, Orsay, France) was used to compensate for ocular aberrations. A custom software control system was used as an interface between the wavefront sensor and deformable mirror. Light reflected from the retina was collected using an avalanche photodiode (APD, model # c5460, Hamamatsu Inc., Japan). A confocal pinhole was used to provide optical sectioning capabilities enabling us to focus on specific layers of the retina (i.e. photoreceptors). A

sample AO-SLO image from a healthy volunteer taken at the University of Texas Medical Branch is shown in Figure 3.

Patients were positioned relative to the incident imaging light source using a micrometer guided headrest with independent controls for the vertical, horizontal and axial positions. For each patient, a sequence of 2°×2° (~0.58 mm × 0.58 mm) raster scans was obtained throughout the macula with particular emphasis on areas of drusen accumulation or geographic atrophy. All image sequences were acquired at a rate of 12 frames per second and a 1024×1024 pixel resolution. Generally, image sequences were acquired for 10–30 seconds at a specified location allowing patients an opportunity to rest intermittently between scans. This prevented eye fatigue and enabled us to evaluate more extensive areas throughout the macula. The power of the SLO beam, measured at the cornea, was <500 μW which is well below the permissible ANSI laser safety level for continuous exposures to the retina. Each AO-SLO imaging session was completed in approximately 30–45 minutes.

Image Processing& Analysis

The video sequences obtained during the imaging procedure were first subjected to a “pre-processing” step in which individual frames exhibiting large motion artifacts due to involuntary eye movement were manually removed. The remaining images were registered using the specialized Fiji platform of ImageJ (originally developed by Wayne Rasband, National Institutes of Health, Bethesda, MD). Briefly, unique features from each image were identified and cross-referenced with subsequent frames in the sequence. Multiple image frames were aligned and averaged to improve the overall signal to noise ratio. An automated stitching algorithm was applied to the imaging sets to generate larger photoreceptor mosaics.

Cone photoreceptor counts were measured using an automated cell identification algorithm, developed by Byun et al., and currently available as an ImageJ plugin(22). Photoreceptor counts were used to generate heat maps to investigate localized changes in cellular density. The heat maps comprised image subsets of 0.25° × 0.25° (128 × 128 pixels) to assess variations in automated cone counting around drusen formation. A comparison of the photoreceptor density for each of the four stages of AMD was performed on a 3° × 1° mosaic from approximately the same region of the macula (~5–7° from the central fovea along the temporal meridian). The change in photoreceptor density across this eccentricity range is only ~30% (from 13k to 10k cones/mm^{223}. Voronoi diagrams were also generated to visualize cellular distribution and identify potential alterations in the cone mosaic.

Results

Current multimodal clinical retinal imaging techniques revealed morphological changes in the retina as a direct result of drusen formation associated with the progression of AMD but provided little insight into the integrity and viability of the macular photoreceptor mosaic. Composite AO-SLO images were used to make a qualitative comparison of retinal morphology between the clinical and investigational retinal imaging systems (Figure 4). AO-SLO imaging revealed a slight disruption in the photoreceptor mosaic in the Category I AMD patient due to focal drusen formation and identified several small drusen deposits that were not observed with standard clinical imaging techniques. The Category II patient exhibited distinct ring shaped areas with reduced reflectance from the photoreceptor layer. These circular patterns correspond with drusen seen using clinical fundus reflectance imaging and SD-OCT. The Category III AMD patient exhibited widespread areas of photoreceptor disruption associated with the extensive coalescent drusen observed clinically. However, we observed large regions of photoreceptors that appeared viable based on the cellular morphology in both Category II and III patients. Consistent with the observations made using the multimodal clinical system, the Category IV AMD patient exhibited

extensive areas of geographic atrophy when imaged with the AO-SLO. However, the high resolution images revealed the presence of sparsely populated photoreceptors in the marginal zones of geographic atrophy. As expected, the advanced AMD patients demonstrated poor central fixation which resulted in a reduction of overall image quality. Despite the dim reflectance and extensive eye movement, images of photoreceptor disruption in the macula from drusen, geographic atrophy and along the margins of RPE atrophy were acquired and analyzed. An increase in photoreceptor disruption was visualized throughout the macula in direct correlation with AMD progression leading to a decrease in central visual acuity (Figure 5).

Measurements of the local photoreceptor density variations revealed areas of suspected degeneration associated with drusen based on a relative decrease in the number of cones identified with the automated algorithm. The automated photoreceptor counts demonstrate a reduced number of reflective cone photoreceptor cells corresponding to the areas of drusen formation and atrophy. The automated algorithm provided a repeatable and unbiased assessment of cellular density regardless of disease category. Photoreceptor counts, heat maps, and Voronoi diagrams from one representative region are shown in Fig. 6 to illustrate localized AMD characteristics. The heat map provides a broad overview of the local variations in photoreceptor density by denoting regions of reduced cell counts in darker colors. Similar to the photoreceptor counts and heat map, the Voronoi diagram provides an additional representation of the photoreceptor mosaic and highlights deviations in the expected cellular packing density which may be beneficial in a clinical setting to assess disease progression.

One-way ANOVA was used to test differences in photoreceptor density among the four clinical stages of AMD. Photoreceptor density was significantly different among the 4 groups ($P < 0.001$). Pairwise multiple comparisons of cone photoreceptor density measurements did not reveal significant differences between Category I and Category II. Similarly, no significant changes in photoreceptor density were noted between Categories III and IV within the region selected for comparison. However, cone density values for Category I were significantly higher than either Category III or IV. Likewise, we counted significantly more cones in Category II compared to Categories III and IV (Table 3). (One-way ANOVA, $P < 0.001$; Pairwise Multiple Comparison – Tukey Test, $P < 0.05$

Discussion

This study demonstrated the use of an investigational adaptive optics retinal imaging system to non-invasively evaluate the pathology of dry age-related macular degeneration at the level of individual photoreceptor cells. AO-SLO provided a complimentary view of the photoreceptor mosaic when combined with the multimodal clinical imaging techniques yielding a highly-detailed assessment of retinal morphology. We were able to quantify local deficits in photoreceptor density associated with the presence of drusen and GA in AMD patients. Based on distinct morphological features, we observed similarities between the disruptions observed with AO-SLO and the multimodal clinical images obtained using NIR reflectance, fundus autofluorescence and SD-OCT.

The presence of an extremely high degree of variability in photoreceptor density at the same retinal eccentricity across multiple subjects is well known (23) . This variability further confounds attempts to assess the spatial distribution of photoreceptors in a diseased retina with substantial morphological alterations, photoreceptor degeneration, and also loss of visual acuity (resulting in poor fixation ability). Therefore, we compared variations in local photoreceptor densities (0.25°×0.25°) across a 3°×1° retinal patch to assess changes with respect to morphological disruption. Subsequent imaging time points in these locations may

provide more detailed information regarding the progressive loss of photoreceptors in AMD. The perifoveal images selected for analysis in the 4 representative cases were chosen because they exhibited characteristic features for their respective AMD categories and were acquired at a similar retinal eccentricity (~5–7° from the central fovea along the temporal meridian). Moreover, atrophy associated with AMD tends to develop first in perifoveal areas(24) which may provide an opportunity to investigate early morphological changes, diagnose patients at earlier time points and implement preventative measures.

Because precise microperimetry or other functional measures did not accompany this structural study, we cannot definitively state that the dark regions in the AO-SLO images indicate atrophy, degeneration, or functional loss. However, histopathologic studies from donor eyes have shown similar disruption of continuity and arrangement in the photoreceptor mosaic in AMD patients(25). Likewise, the complimentary clinical imaging techniques support this conclusion based on disruption observed in SD-OCT cross-sections. Most notably, a reduction in the reflective layer associated with the junction between the inner and outer photoreceptor segments (IS/OS) was absent or substantially reduced in the immediate vicinity of drusen formation or GA. Fundus autofluorescence images also provided some insight into the health and viability of the RPE and photoreceptors in regions with pigment abnormalities and signs of atrophy.

Despite the technical challenges of imaging older patients with low vision and difficulty maintaining fixation for extended periods of time, AO-SLO has revealed an unprecedented view of the effects of dry age-related macular degeneration *in vivo*. These challenges were overcome by obtaining multiple 2°×2° raster scans throughout the macula with particular emphasis placed on areas of drusen formation or geographic atrophy. Averaging multiple frames to improve the signal-to-noise ratio was a necessary step to suppress background noise and minor motion artifacts prior to analysis. In addition to obtaining large data sets representing multiple areas throughout the macula, we used a relatively large confocal pinhole (400 μm diameter) to acquire the image sequences in each AMD patient. Although this resulted in the admittance of additional scattered light and a decrease in both axial and lateral resolution, this trade-off was necessary to obtain sufficient signal reflected from the maculae of our patients. Additionally, the larger confocal pinhole enabled us to image areas of substantial focal distortion as large drusen were shown to push the RPE and photoreceptors upward. As a final step, the averaged images were stitched together to create the larger photoreceptor mosaics within the macula.

As part of this ongoing study, we plan to follow these patients annually to monitor alterations in the photoreceptor mosaic as a result of AMD progression. By conducting a longitudinal study to examine localized changes in photoreceptor density, we hope to identify characteristic features of disease progression. Future studies would benefit from faster image acquisition speed and more advanced retinal tracking to minimize the effects of involuntary eye movements. New adaptive optics retinal imaging systems have also demonstrated heightened capabilities which enable differentiation between rod and cone photoreceptors in healthy volunteers(26,27). This would be particularly appealing in AMD patients as rod photoreceptors have been shown to degenerate in the perifoveal area prior to cones(25). Furthermore, application of AO-SLO may provide insight into current therapies for advanced AMD, such as photocoagulation, photodynamic therapy and intravitreal injections. Likewise, AO-SLO may be used to examine the benefits of emerging therapies for early AMD.

Conclusion

We have successfully demonstrated the use of adaptive optics retinal imaging in patients with dry AMD to obtain an unprecedented view of the disrupted photoreceptor mosaic *in vivo*. There are numerous investigational and clinical applications for adaptive optics in the field of ophthalmology. Current diagnostic instruments are limited to a wider view of the fundus; a more detailed assessment of retinal pathology with high resolution adaptive optics imaging techniques may help improve diagnostic accuracy and long term treatment strategy. Moreover, AO retinal imaging may be used as an adjunct method to validate the efficacy of emerging dry AMD therapies that are currently undergoing clinical trials.

Acknowledgments

We would like to acknowledge Ryan Harris and Mark Stephens for their assistance with patient recruitment. This work was supported in part by, the American Society for Laser Medicine & Surgery (ASLMS) Student Research Grant, The Wagner AMD Fund, Seymour Fisher, the Institute for Translational Sciences at the University of Texas Medical Branch, Research to Prevent Blindness (RPB) and CTSA NIH Grant.

References

1. Rein DB, Wittenborn JS, Zhang X, Honeycutt AA, Lesesne SB, Saaddine J. Group VHC-ES. Forecasting age-related macular degeneration through the year 2050: the potential impact of new treatments. Arch Ophthalmol. 2009; 127(4):533–540. [PubMed: 19365036]
2. Klein R, Chou CF, Klein BE, Zhang X, Meuer SM, Saaddine JB. Prevalence of age-related macular degeneration in the US population. Arch Ophthalmol. 2011; 129(1):75–80. [PubMed: 21220632]
3. Klein R, Klein BE, Linton KL. Prevalence of age-related maculopathy. The Beaver Dam Eye Study. Ophthalmology. 1992; 99(6):933–943. [PubMed: 1630784]
4. Holz FG, Bellman C, Staudt S, Schütt F, Völcker HE. Fundus autofluorescence and development of geographic atrophy in age-related macular degeneration. Invest Ophthalmol Vis Sci. 2001; 42(5): 1051–1056. [PubMed: 11274085]
5. Fleckenstein M, Charbel Issa P, Helb HM, Schmitz-Valckenberg S, Finger RP, Scholl HP, Loeffler KU, Holz FG. High-resolution spectral domain-OCT imaging in geographic atrophy associated with age-related macular degeneration. Invest Ophthalmol Vis Sci. 2008; 49(9):4137–4144. [PubMed: 18487363]
6. Curcio CA, Owsley C, Jackson GR. Spare the rods, save the cones in aging and age-related maculopathy. Invest Ophthalmol Vis Sci. 2000; 41(8):2015–2018. [PubMed: 10892836]
7. Curcio CA, Medeiros NE, Millican CL. Photoreceptor loss in age-related macular degeneration. Invest Ophthalmol Vis Sci. 1996; 37(7):1236–1249. [PubMed: 8641827]
8. Porter, J. Adaptive optics for vision science : principles, practices, design, and applications. Hoboken, NJ: Wiley-Interscience; 2006.
9. Liang J, Williams DR, Miller DT. Supernormal vision and high-resolution retinal imaging through adaptive optics. J Opt Soc Am A Opt Image Sci Vis. 1997; 14(11):2884–2892. [PubMed: 9379246]
10. Roorda A, Romero-Borja F, Donnelly Iii W, Queener H, Hebert T, Campbell M. Adaptive optics scanning laser ophthalmoscopy. Opt Express. 2002; 10(9):405–412. [PubMed: 19436374]
11. Zhang Y, Poonja S, Roorda A. MEMS-based adaptive optics scanning laser ophthalmoscopy. Opt Lett. 2006; 31(9):1268–1270. [PubMed: 16642081]
12. Burns SA, Tumbar R, Elsner AE, Ferguson D, Hammer DX. Large-field-of-view, modular, stabilized, adaptive-optics-based scanning laser ophthalmoscope. J Opt Soc Am A Opt Image Sci Vis. 2007; 24(5):1313–1326. [PubMed: 17429477]
13. Miller DT, Kocaoglu OP, Wang Q, Lee S. Adaptive optics and the eye (super resolution OCT). Eye (Lond). 2011; 25(3):321–330. [PubMed: 21390066]
14. Zhang Y, Cense B, Rha J, Jonnal RS, Gao W, Zawadzki RJ, Werner JS, Jones S, Olivier S, Miller DT. High-speed volumetric imaging of cone photoreceptors with adaptive optics spectral-domain optical coherence tomography. Opt Express. 2006; 14(10):4380–4394. [PubMed: 19096730]

15. Zawadzki RJ, Choi SS, Jones SM, Oliver SS, Werner JS. Adaptive optics-optical coherence tomography: optimizing visualization of microscopic retinal structures in three dimensions. J Opt Soc Am A Opt Image Sci Vis. 2007; 24(5):1373–1383. [PubMed: 17429483]

16. Mujat M, Ferguson RD, Patel AH, Iftimia N, Lue N, Hammer DX. High resolution multimodal clinical ophthalmic imaging system. Opt Express. 2010; 18(11):11607–11621. [PubMed: 20589021]

17. Song H, Chui TY, Zhong Z, Elsner AE, Burns SA. Variation of cone photoreceptor packing density with retinal eccentricity and age. Invest Ophthalmol Vis Sci. 2011; 52(10):7376–7384. [PubMed: 21724911]

18. Chui TY, Song H, Burns SA. Adaptive-optics imaging of human cone photoreceptor distribution. J Opt Soc Am A Opt Image Sci Vis. 2008; 25(12):3021–3029. [PubMed: 19037393]

19. Li KY, Tiruveedhula P, Roorda A. Intersubject variability of foveal cone photoreceptor density in relation to eye length. Invest Ophthalmol Vis Sci. 2010; 51(12):6858–6867. [PubMed: 20688730]

20. Chui TY, Song H, Burns SA. Individual variations in human cone photoreceptor packing density: variations with refractive error. Invest Ophthalmol Vis Sci. 2008; 49(10):4679–4687. [PubMed: 18552378]

21. Klein ML, Ferris FL, Armstrong J, Hwang TS, Chew EY, Bressler SB, Chandra SR, Group AR. Retinal precursors and the development of geographic atrophy in age-related macular degeneration. Ophthalmology. 2008; 115(6):1026–1031. [PubMed: 17981333]

22. Byun J, Verardo MR, Sumengen B, Lewis GP, Manjunath BS, Fisher SK. Automated tool for the detection of cell nuclei in digital microscopic images: application to retinal images. Mol Vis. 2006; 12:949–960. [PubMed: 16943767]

23. Curcio CA, Sloan KR, Kalina RE, Hendrickson AE. Human photoreceptor topography. J Comp Neurol. 1990; 292(4):497–523. [PubMed: 2324310]

24. Sarks JP, Sarks SH, Killingsworth MC. Evolution of geographic atrophy of the retinal pigment epithelium. Eye (Lond). 1988; 2(Pt 5):552–577. [PubMed: 2476333]

25. Curcio CA. Photoreceptor topography in ageing and age-related maculopathy. Eye (Lond). 2001; 15(Pt 3):376–383. [PubMed: 11450761]

26. Doble N, Choi SS, Codona JL, Christou J, Enoch JM, Williams DR. In vivo imaging of the human rod photoreceptor mosaic. Opt Lett. 2011; 36(1):31–33. [PubMed: 21209677]

27. Dubra A, Sulai Y, Norris JL, Cooper RF, Dubis AM, Williams DR, Carroll J. Noninvasive imaging of the human rod photoreceptor mosaic using a confocal adaptive optics scanning ophthalmoscope. Biomed Opt Express. 2011; 2(7):1864–1876. [PubMed: 21750765]

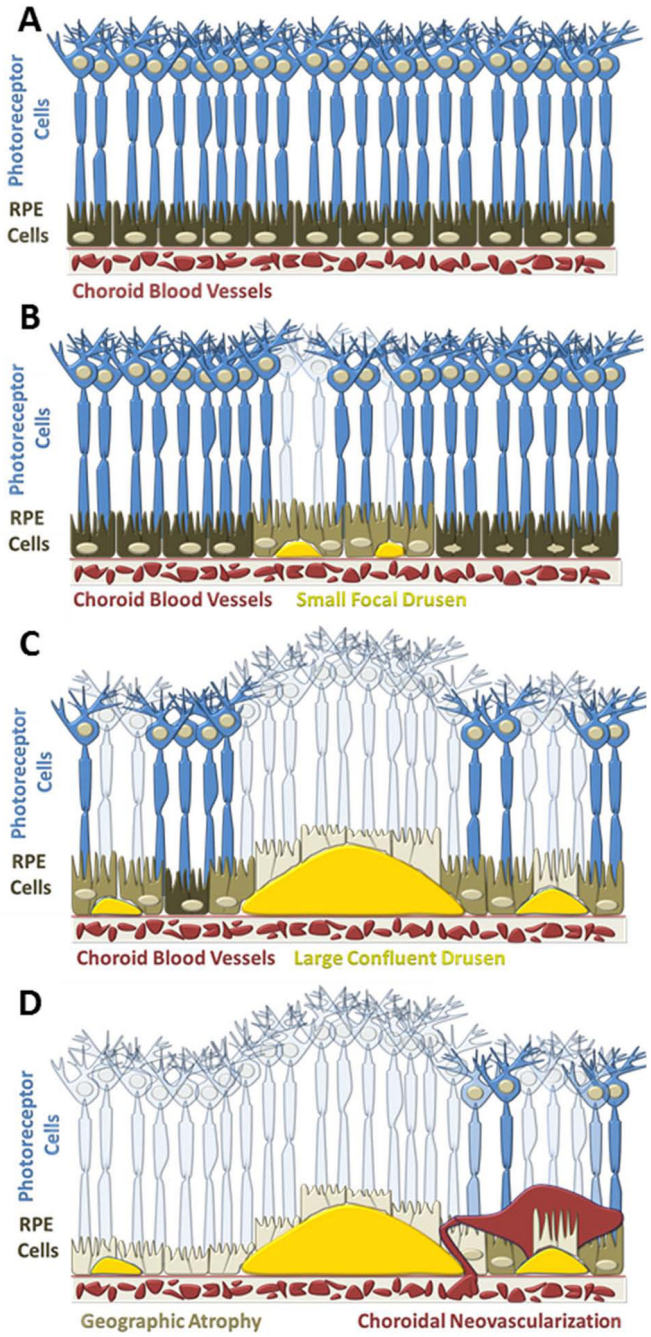

Figure 1.
Cartoon depiction of AMD progression (A) Healthy retina exhibiting a uniform photoreceptor mosaic (B) Early signs of AMD represented by small focal drusen in the sub-RPE space causing minimal disruption of the overlying photoreceptor cells. (C) Intermediate AMD with larger confluent drusen and more extensive loss of photoreceptor cells (D) Advanced AMD exhibiting extensive central geographic atrophy of the RPE cells and choroidal neovascularization.

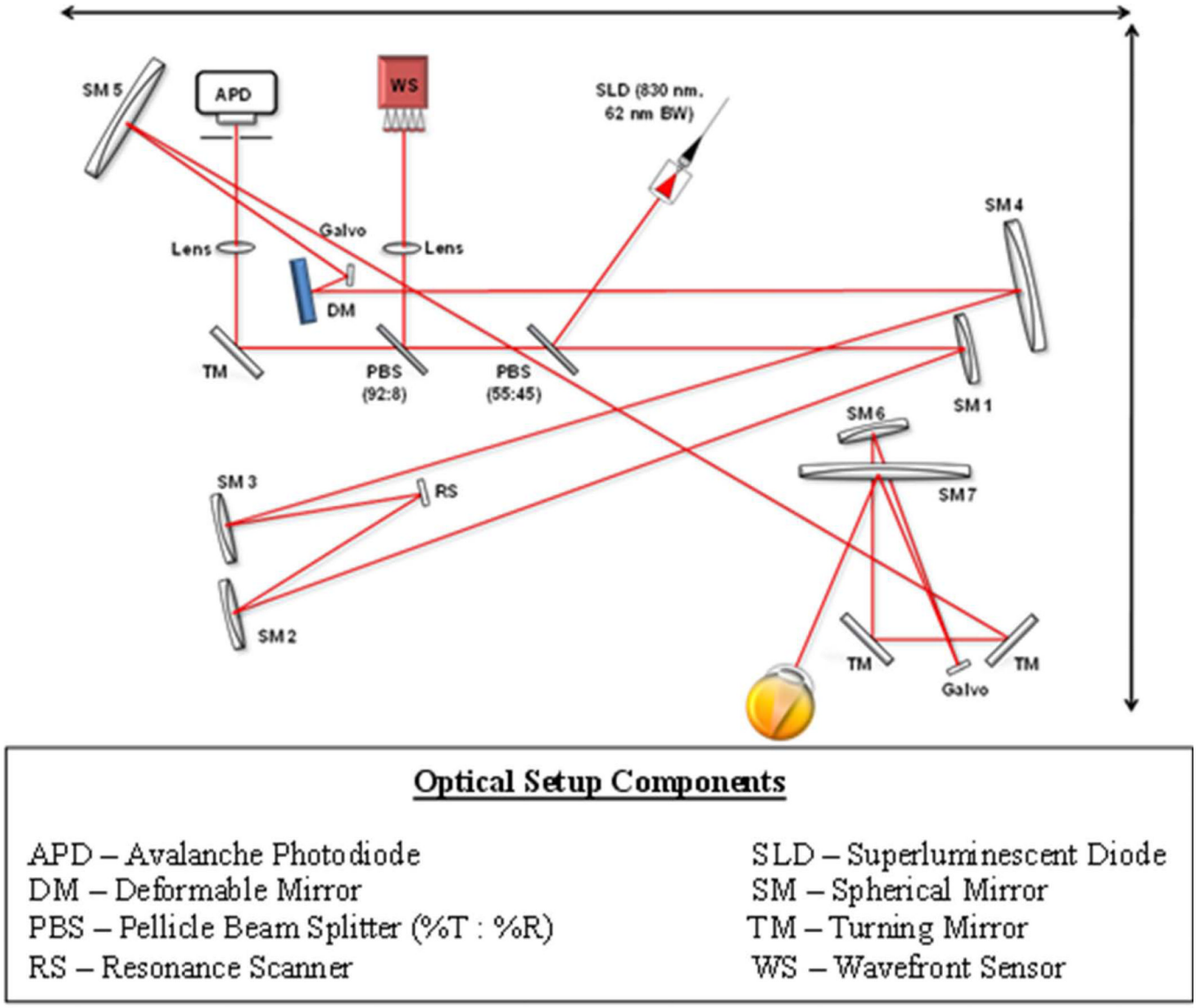

Figure 2.
Diagram of the general optical layout of the AO-SLO. All optical elements are confined to a 2’ × 2’ breadboard while patients are seated and positioned using a micrometer guided headrest (diagram not to scale). A list of the optical and sensing elements is shown below the diagram.

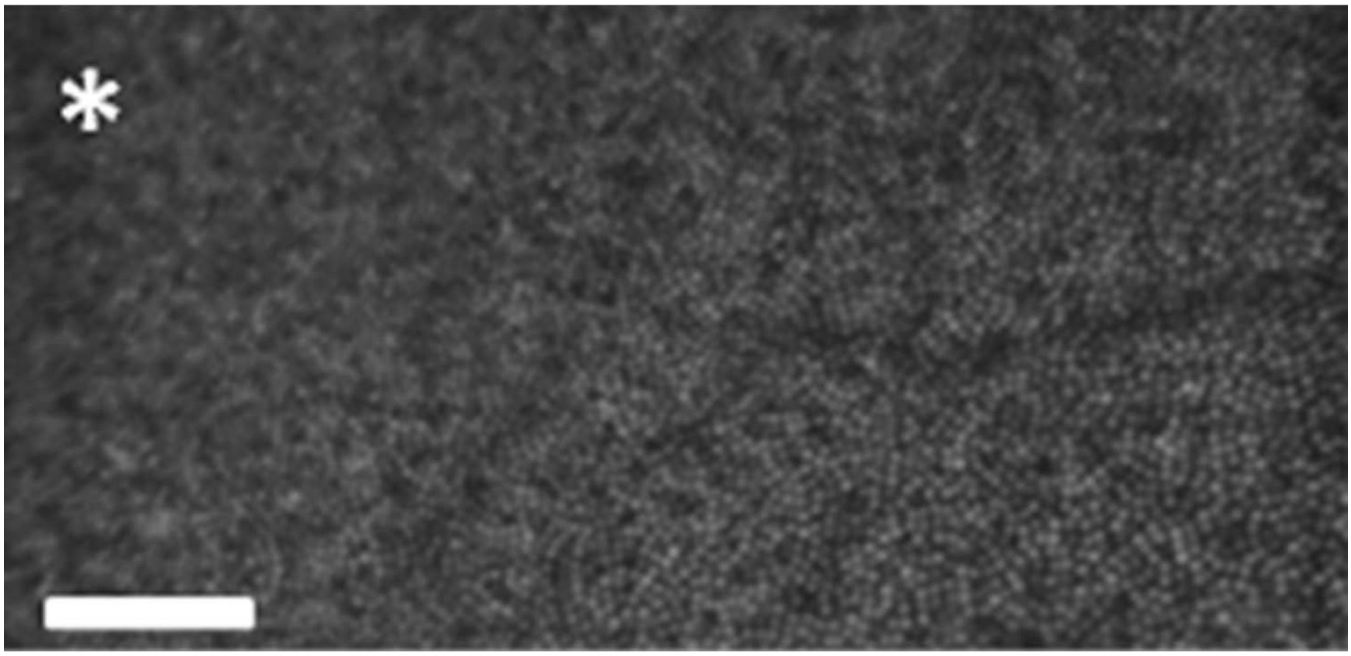

Figure 3.
Cone photoreceptor image (2° × 1°, ~0.58 mm × 0.29 mm) acquired from a healthy volunteer using the AO-SLO at the University of Texas Medical Branch. The cone photoreceptors immediately adjacent to the fovea exhibit the typical circular shape, bright reflectance and normal packing density [Scale bar = 0.1mm, asterisk marks the center of the fovea]

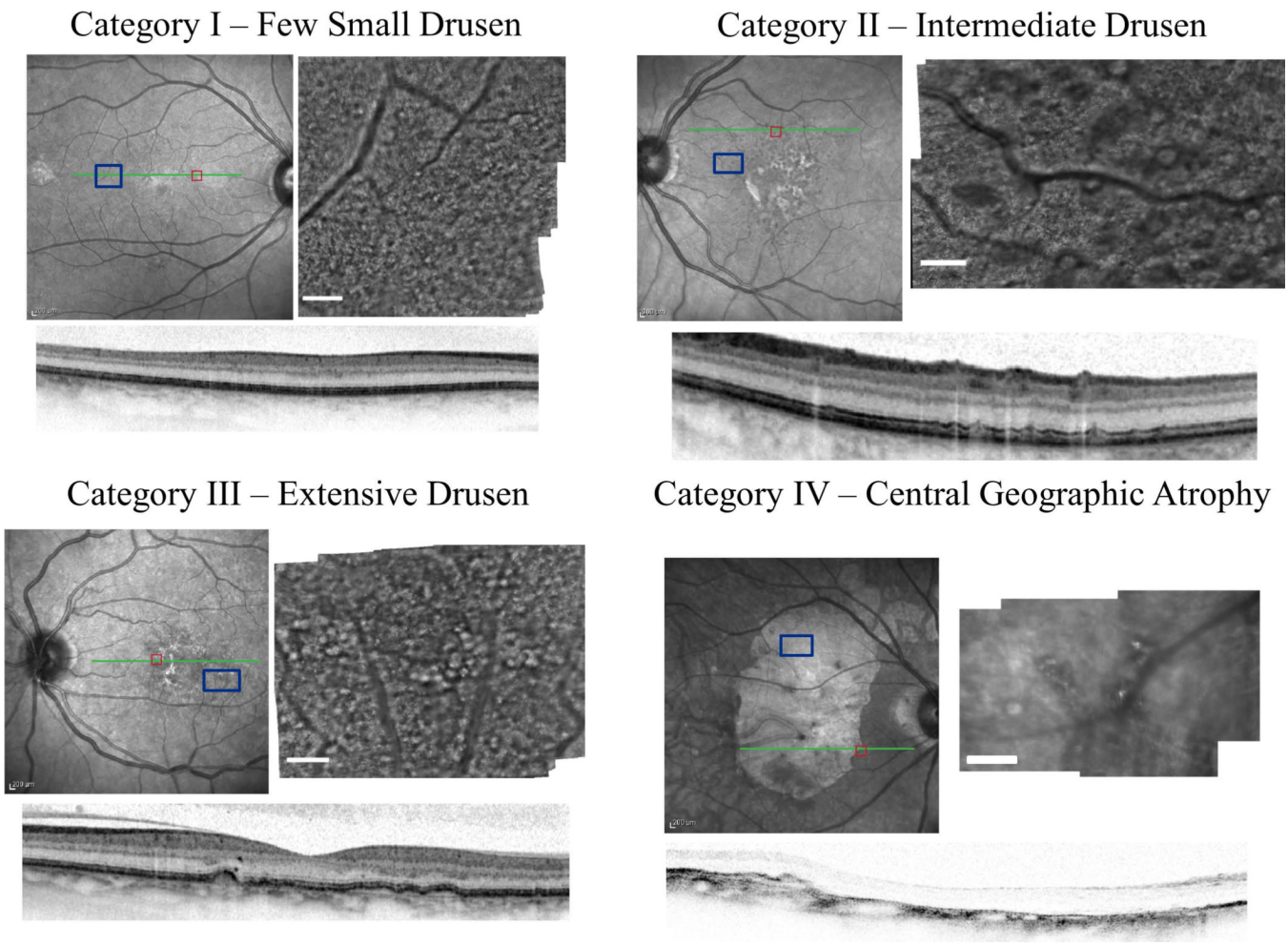

Figure 4.

Wide field (30° × 30°) near infrared fundus reflectance images with corresponding Spectral Domain Optical Coherence Tomography cross-sections (position noted by the horizontal green line) provides an overview of the retinal morphology for each patient. AO-SLO cone photoreceptor mosaics shown are represented by the blue rectangles. The small scale of the images demonstrates the effect of disease progression on cone photoreceptors for a representative patient from each category (red rectangles represent additional scan areas – *not shown*) Scale bars represent 200 μm

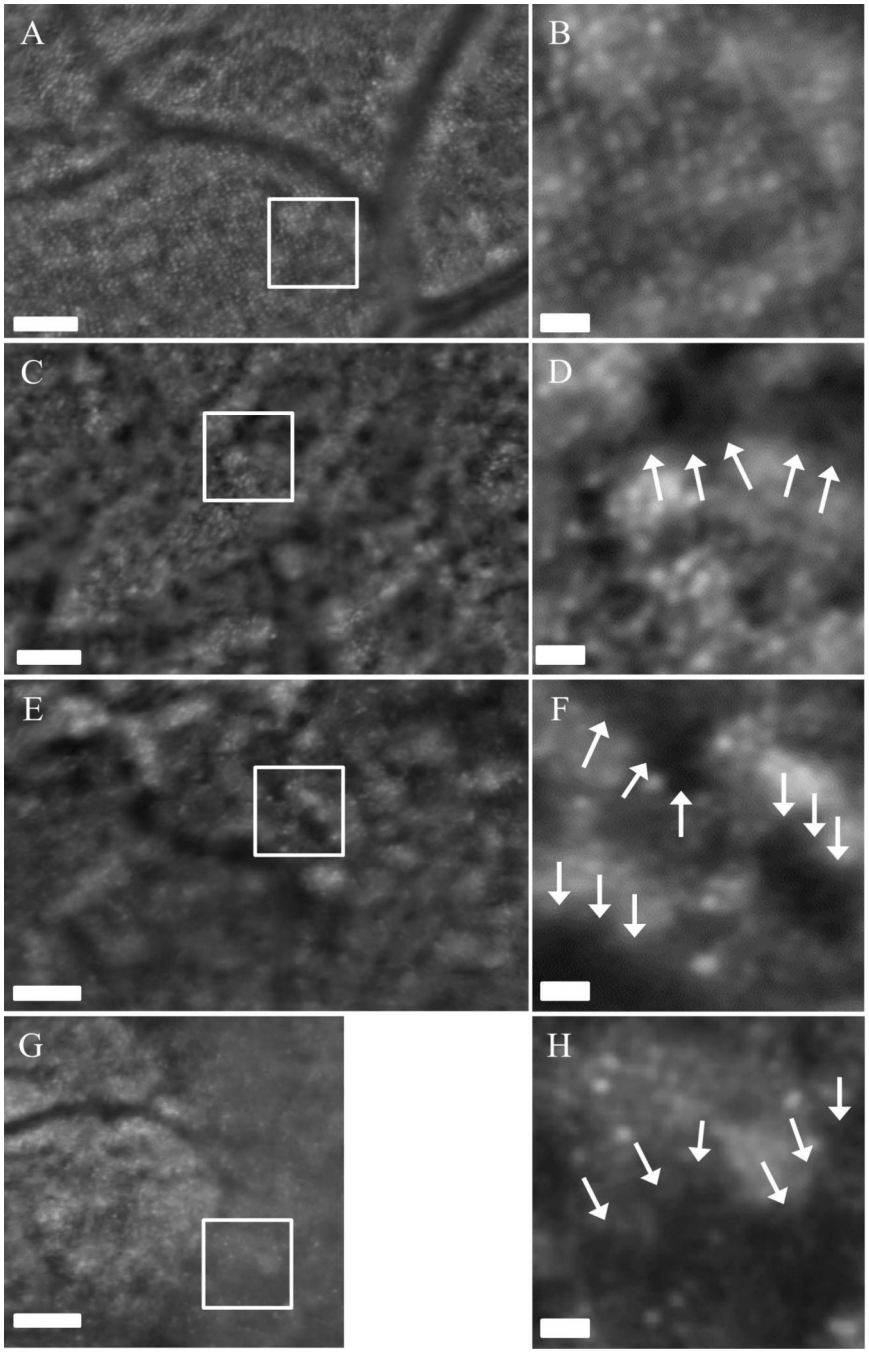

Figure 5.
AO-SLO composite images from Category I patient (A, B), Category II (C, D), Category III (E, F) and Category IV (G, H). White boxes represent the 0.5°×0.5° regions shown in B, D, F & H. An increase in photoreceptor disruption can be observed as a function of disease progression. The arrows denote regions with decreased reflectance possibly indicating loss of functionality or atrophy of cone photoreceptors. Scale bars (A, C, E, & G) = 0.1 mm. Scale bars (B, D, F, & H) = 0.02 mm

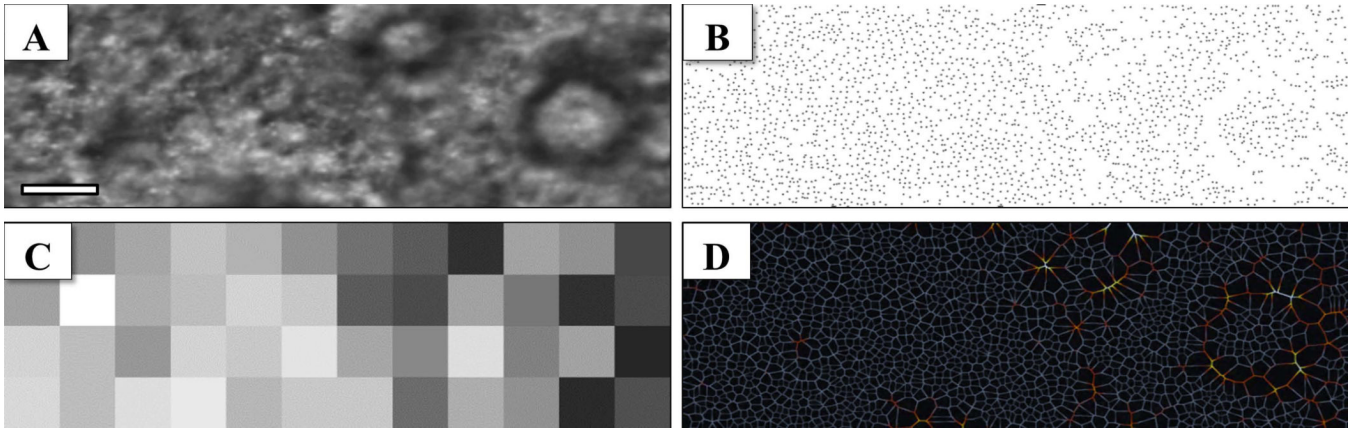

Figure 6.

Example of cone photoreceptor density analysis from a Category II dry AMD patient (A) cone photoreceptor mosaic (3° × 1°, ~ 0.87 mm × 0.29 mm) (B) Automated identification of cone photoreceptor locations reveal areas of suspected degeneration or loss of functionality (C) Heat map of localized photoreceptor densities in 0.25° × 0.25° regions to provide a broad assessment of changes associated with AMD, dark regions represent lower relative photoreceptor density [values range from 2568 – 13983 cones/mm^2; mean value ± SD: 8698 ± 2964] (D) Voronoi diagram demonstrating the relationship between photoreceptor packing density and alterations caused by drusen formation. Deviations in the expected cellular organization can easily be seen using these complimentary depictions. [Scale bar = 0.1 mm]

Table 1

Characterization of AMD based on the appearance of drusen using standard fundus photography methods.

Age-Related Eye Disease Study (AREDS) Stages of AMD	
Category I	No or few small drusen (<63 μm)
Category II	Intermediate drusen (<125 μm)
Category III	Extensive intermediate or large drusen (>125 μm)
Category IV	Neovascular AMD or Central Geographic Atrophy

Table 2

Summary of Patient Demographics

Current Patient Population			
	Eye Imaged	***Age***	***Visual Acuity***
Patient 1 (Category I)	OD	74	20/25
Patient 2 (Category II)	OS	77	20/30
Patient 3 (Category III)	OS	65	20/25
Patient 4 (Category IV)	OD	86	CF 2 ft *

OD – right eye, OS – left eye.

* Patient was only able to count the examiners fingers at a distance of two feet.

Table 3

Cone photoreceptor density analysis for a representative patient from each AMD category

	n	Mean Cone Density [Cones/mm^2]	Standard Deviation	Min	Max
Category I	48	9128	± 1612	4946	14269
Category II	48	8698	± 2965	2568	13983
Category III	48	5443	± 1259	3234	8371
Category IV	48	4744	± 1377	1141	7420

Multiple Comparisons (Tukey Test)	
Category I vs Category IV	P < 0.05
Category I vs Category III	P < 0.05
Category I vs Category II	No
Category II vs Category IV	P < 0.05
Category II vs Category III	P < 0.05
Category III vs Category IV	No

One-way ANOVA was used to test differences in photoreceptor density among the four clinical stages of AMD. Photoreceptor density was significantly different among the 4 groups ($P < 0.001$). Post-hoc comparison of the groups (Tukey Test) found Category I to have a significantly higher cone density than both Category III & IV. Likewise, Category II demonstrated significantly higher cone density than both Category III & IV. No significant differences were observed between Category I & II or between Category III & IV (values were deemed significant at $P < 0.05$).Composite images for each patient represent ~5–7° from the central fovea along the temporal meridian. Each data point represents a 0.25°×0.25° region to assess local variations in cone density.